Canadian Journal of Pure and Applied Sciences
Vol. 16, No. 2, pp. 5475-5482, June 2022
Online ISSN: 1920-3853; Print ISSN: 1715-9997
Available online at www.cjpas.net

SCALAR POTENTIAL MODEL OF THE PIONEER ANOMALY

John C. Hodge
Blue Ridge Community College, 100 College Dr., Flat Rock, NC 28731-7756, USA

ABSTRACT

The unexplained sunward acceleration (a_P) of the Pioneer 10 (P10) and the Pioneer 11 (P11) spacecrafts remains a mystery. A scalar potential model (SPM) that derived from considerations of galaxy clusters, redshift, and HI rotation curves of spiral galaxies is applied to the Pioneer Anomaly. Matter is posited to warp the scalar potential ρ field. The changing ρ field along the light path causes the Pioneer Anomaly. The SPM is consistent with the general value of the a_P; with the annual periodicity; with the differing a_P between the spacecrafts; with the discrepancy between Sigma and CHASMP programs at P10 (I) and their closer agreement at P10 (III); with the slowly declining a_P; with the low value of the a_P immediately before the P11's Saturn encounter; with the high uncertainty in the value of the a_P obtained during and after the P11's Saturn encounter; and with the cosmological connection suggested by $a_P \approx cH_o$. The effect of the ρ field warp appears as the curvature of space proposed by the general relativity (GR). The Hubble Law and $a_P \approx cH_o$ are manifestations of the Newtonian spherical property. Therefore, gravitational attraction, the equivalence principle, and the planet ephemeris remain as described by the GR. The GR corresponds to the SPM in the limit in which the Sources and Sinks may be replaced by a flat and static ρ field such as between cluster cells and on the Solar System scale at a relatively large distance from a Source or Sink.

Keywords: Pioneer anomaly, Gravity tests, cosmology.
PACS numbers: 04.80.Cc, 95.30.Sf, 98.80.-h

INTRODUCTION

That an unexplained blueshift exists in the electromagnetic (EM) radio signal from the Pioneer 10 (P10) and Pioneer 11 (P11) (Pioneer Anomaly) is well established (Anderson *et al*., 2002; Toth and Turyshev, 2006). Several models have been proposed to explain the Pioneer Anomaly (Anderson *et al*., 2002), see also in (Iorio and Gioudice, 2006; Nieto and Anderson, 2005; Nieto *et al*., 2005; Turyshev *et al*., 1999). A currently popular interpretation of the Pioneer Anomaly (PA) is that the Pioneer spacecrafts are being subjected to a force that causes a sunward acceleration $a_P \approx (8.74 \pm 1.33) \times 10^{-8}$ cm s^{-2}. That $a_P \approx cH_o$, where c (cm s^{-1}) is the speed of light and H_o (s^{-1}) is the Hubble constant, suggests a cosmological connection to the PA. However, the PA exceeds by at least two orders of magnitude the general relativity (GR) corrections to the Newtonian motion.

The PA is experimentally observed as a frequency shift but expressed as an apparent acceleration. The PA can be an effect other than a real acceleration such as a time acceleration (Anderson *et al*. 2002; Nieto and Anderson, 2005) or an effect of an unmodeled effect on the radio signals. Although unlikely, a currently unknown systematics effect is not entirely ruled out.

The data for the existence of the a_P from the Galileo, Ulysses, Voyager, and Cassini spacecrafts are inconclusive (Anderson *et al*., 2002; Nieto *et al*., 2005).

In addition to the Sun directed blueshift, there are other characteristics of the PA (Anderson *et al*., 2002). The PA has an apparent annual periodicity with an amplitude of approximately 1.6×10^{-8} cm s^{-2}. Although within uncertainty limits, the P11 anomaly $a_{P11} \approx 8.55 \times 10^{-8}$ cm s^{-2} may be slightly larger than the P10 anomaly $a_{P10} \approx 8.47 \times 10^{-8}$ cm s^{-2} (Anderson *et al*., 2002, Section V.A., Section VI.A., Section VI.D., and Section VIII.G.). The a_P calculations by the Sigma and CHASMP program methods for P10 (I) and P10 (II) show a discrepancy while showing consistency for P10 (III) (Anderson *et al*., 2002, Table I). The a_P of both spacecraft may be declining with distance (Turyshev *et al*., 1999; as shown by the envelope in Figure 1). The blue shift of the PA is significantly smaller (Nieto and Anderson, 2005) immediately before P11's Saturn encounter. The value of the a_P averaged over a period during and after the Saturn encounter had a relatively high uncertainty (Nieto and Anderson, 2005).

Corresponding author e-mail: jchodge@frontier.com

An obstacle to a new gravitational physics explanation of the PA is that a modification of gravity large enough to explain the PA is in contradiction to planetary ephemeredes unless the Equivalence principle is violated (Anderson *et al*., 2002). The common opinion is that cosmic dynamics according to the GR has far too little influence in galaxies to be measurable and that the expansion of the universe is essentially negligible for scales up to galactic clusters (Cooperstock *et al*., 1998; Sellwood and Kosowsky, 2001). Further, the expansion of the universe indicated by redshift *z* has a sign opposite to the a_P. Several new physics models have been proposed (Anderson *et al*., 2002; Bertolami and Páramos, 2004). Bertolami and Páramos (2004) concluded a scalar field is able to explain the PA.

A scalar potential model (SPM) was derived from considerations of galaxy clusters (Hodge, 2006). The SPM posits a scalar potential ρ field exists. The Sources of the ρ field are in the center of spiral galaxies. Sinks are in elliptical and other galaxies. The ρ field was posited to flow from Sources to Sinks like heat or fluid. The SPM proposed the ρ field caused a non-Doppler redshift or blueshift of photons traveling through it. The resulting equation was applied to *z* and discrete redshift of galaxies.

This paper argues that matter causes a static, nonflowing warp of the ρ field that causes the PA. The $\rho \propto -R^{-1}$ of the warp induces the H_o value and the connection to the *z* observations. That is, the PA is an unaccounted effect on only the EM signal. Therefore, gravitational attraction, the equivalence principle, and the planet ephemeris remain as described by the GR.

In the following section, the SPM is described and an equation to calculate the a_P is derived. The derived equation is used to calculate the a_P in the third section. The discussion and conclusion are in the fourth section.

THE MODEL

In addition to the propositions of the SPM, matter is posited to cause a static warp in the ρ field in accordance with the Newtonian spherical property. ("Static" such as caused by a stationary electron in a stationary EM field. Sources induce a flow such as a source of heat or fluid.) Because the ρ field near matter must attract other matter, the matter decreases the ρ field. The ρ field then causes matter attraction according to established gravitational physics and causes the frequency change of the EM signal. "Static" because matter is neither a Source nor a Sink of energy. Matter merely modifies the energy flowing from Sources to Sinks. The PA is an effect on only the EM signal and is a blueshift superimposed on the Doppler redshift of the receding spacecraft.

The amount of warp ρ_m at a point in space was posited to be equal to GM/R, where G is the Newtonian gravitational constant, M is the mass of a body, and R is the distance from the center of mass to the point where ρ is calculated. That is,

$$\rho_m = -\sum_i^N GM_i / R_i \quad (1)$$

where N is the number of bodies used in the calculation.

The K_{min} term in the equation derived by Hodge (2006) resulted from the flow from Sources. The K_{vp} term results from the relative movement of galaxies. Therefore, $K_{min} = 0$ and $K_{vp} = 0$ for the static warp field of matter in the Solar System. Because the K factors were calculated in a flowing ρ field, the static warp requires other values of the K factors. The resulting equation for the calculated redshift z_c is

$$z_c = e^{-X} - 1 \quad (2)$$

where

$$X = K_{dp} D_1 P + K_p P + K_f F \quad (3)$$

In expression (3), the terms are defined by Hodge (2006), $D_l = 2D$ (AU) is the distance the radio signal travels, and D (AU) is the geocentric distance to the spacecraft. The P is a measure of the amount of ρ the EM signal travels through. The F is a measure of the inhomogeneity (turbulence) of ρ the EM signal travels through. These factors K_{dp}, K_p, and K_f are listed in Table 1.

Table 1. The values of the constants of Equation (2).

Parameter	Value	Units
K_{dp}	1.30×10^{-28}	$erg^{-1}\ AU^{-2}$
K_p	2.10×10^{-26}	$erg^{-1}\ AU^{-1}$
K_f	5.38×10^{-22}	erg^{-1}
K_{co}	-5.98×10^{6}	$erg\ AU^{-1}$

THE RESULTS

The sample

The mass of the Kuiper belt of approximately 0.3 Earth masses (Teplitz *et al*., 1999) and the asteroid belt of approximately one Earth mass were included in the mass of the Sun. The ephemeris including GM of the Sun, planets, dwarf planets, and the moons of the Saturn were obtained from JPL's Horizon website (http://ssd.jpl.nasa.gov/horizons.cgi) in November and December, 2006. The planets barycenter data were used for the calculation except for the Earth and its moon and except when considering the Saturn encounter of P11. When considering the Saturn encounter, the GM of the moons of the Saturn without the GM data in the Horizon

website were calculated from the relative volume and mass of the other moons of the Saturn. The data were taken from the ephemeris for 00^h00^m of the date listed except for the Saturn encounter where hourly data were used.

The a_P data were obtained from Table 2 of Nieto and Anderson (2005). The calculation of ρ starting from the surface of the Earth along the line-of-sight (LOS) to the position of the spacecraft and back used a Visual Basic program. Note the calculation of F is direction dependent. The Galaxy's effective mass was calculated from the revolution of the Sun about the center of the Galaxy and, for simplicity, assumed a spherically symmetric galactic matter distribution. For the calculations, the Galaxy center of mass was positioned at 8 kpc from the Sun in the direction of Sgr A*. The ρ field due to the Source was assumed to be flat across the solar system. Therefore, the effective mass at the center of the galaxy accounts for both the variation of ρ from the Source and the true mass within the Galaxy (Hodge, 2022. Scalar potential model of spiral galaxy HI rotation curves and rotation curve asymmetry. Canadian Journal of Pure and Applied Sciences. 16(2):In Press).

Equation (2) was used to calculate the z_c for each spacecraft on each date. The calculated PA acceleration a_{Pc} (cm s^{-2}) (Anderson *et al*., 2002) is

$$a_{\mathrm{Pc}} = -c^2 z_{\mathrm{c}} / D_l \tag{4}$$

The components of the z_c values are listed in Table 2. Figure 1 shows the plots of the a_P and a_{Pc} values versus the D for each spacecraft. The correlation coefficient between the a_P and a_{Pc} is 0.85 for all data points. Without the P11 80/66 data point, which is the most uncertain measurement (Nieto and Anderson, 2005), the a_P and a_{Pc} correlation coefficient is 0.93.

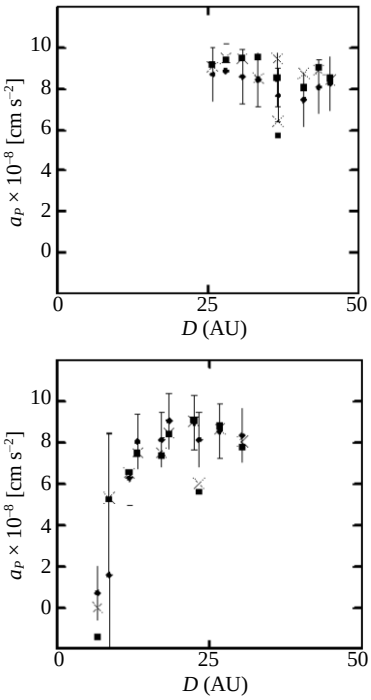

Fig. 1. The plots of the a_P data versus the geocentric distance D for P10 (upper figure) and P11 (lower figure). The solid diamonds reflect the a_P from Nieto and Anderson (2005), the solid squares are the calculated points for the a_{Pc}, and the "X's" are calculated points for dates ten days from the date of the a_P.

The error bars in Figure 1 reflect the uncertainty from Table 2 of Anderson *et al*. (2002) except for P11 80/66

Table 2. The components of Equation (2) and A_{sun} for each data point.

Craft Date		D (AU)	$K_{\mathrm{dp}}DP \times 10^{-14}$	$K_{\mathrm{p}}P \times 10^{-14}$	$K_{\mathrm{f}}F \times 10^{-14}$	$X \times 10^{-13}$	A_{sun} (°)
P10 82/19		25.80	-1.83	-5.74	15.40	0.78	124
P10 82/347		27.93	-2.06	-5.97	16.77	0.87	165
P10 83/338		30.68	-2.43	-6.42	18.54	0.97	167
P10 84/338		33.36	-2.82	-6.85	20.27	1.06	175
P10 85/138		36.57	-4.43	-9.81	21.17	0.69	12
P10 86/6		36.53	-3.34	-7.42	21.12	1.04	144
P10 87/80		40.92	-4.38	-8.66	23.96	1.09	70
P10 88/68		43.34	-4.76	-8.90	26.69	1.30	82
P10 89/42		45.37	-5.04	-8.99	26.82	1.28	109
P11 77/270		6.49	-0.24	-3.05	2.99	-0.03	43
P11 80/66		8.42	-0.26	-2.49	4.23	0.15	166
P11 82/190		11.80	-0.49	-3.34	6.41	0.26	109
P11 83/159		13.13	-0.55	-3.42	7.25	0.33	148
P11 84/254		17.13	-0.99	-4.68	9.83	0.42	71
P11 85/207		18.36	-1.01	-4.47	10.62	0.51	121
P11 86/344		23.19	-2.09	-7.31	13.74	0.43	16
P11 87/135		22.41	-1.40	-5.06	13.23	0.68	151
P11 88/256		26.62	-2.01	-6.12	15.93	0.78	88
P11 89/316		30.29	-2.85	-7.62	18.29	0.78	36

where the uncertainty is from Nieto and Anderson (2005). The stochastic variable of the unmodeled acceleration was sampled in ten-day or longer batches of data (Anderson *et al*., 2002). Starting at the P11 80/66 data point, the average extended over many months (Nieto and Anderson, 2005). The "X's" shown in Figure 1 plot the calculated data point for a ten-day change from the date of the a_P. Some data points showed little change between the two dates of calculation. Others showed moderate change. Because the value of a_{Pc} depends on the closeness of matter to the LOS, a change over ten days is due to a body close to the LOS and to long integration times. Therefore, the closeness of matter to the LOS introduces an uncertainty for even ten-day integration times that was unaccounted in the error budget.

The a_{Pc} calculation reproduces the subtler effects of the PA noted by Anderson *et al*. (2002).

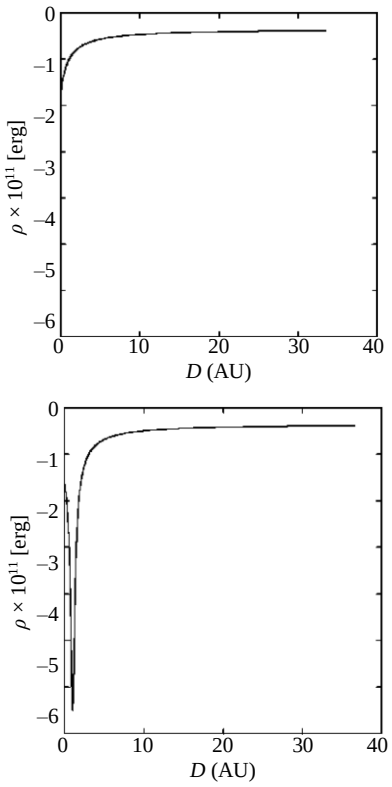

Fig. 2. The plots of the ρ versus the geocentric distance D along the LOS. These data are for P10 on 84/338 (upper figure) $a_P = 8.43 \times 10^{-8}$ cm s^{-2} and for P10 on 85/138 (lower figure) $a_P = 7.67 \times 10^{-8}$ cm s^{-2}. The $A_{sun} \approx 175°$ on P10 84/338 and $A_{sun} \approx 16°$ on P10 85/138.

Annual periodicity

Figure 2 shows the ρ value along the LOS versus the D on dates when the angle A_{sun} (degrees) between the LOS and a line from the Earth to the Sun was < 60° and when A_{sun} > 120°.

Table 2 lists the A_{sun} for each data point. On the dates that A_{sun} < 60°, the a_P and a_{Pc} were considerably lower. The correlation coefficient between the a_P and a_{Pc} without P10 85/138 ($A_{sun} \approx 12°$), P11 86/344 ($A_{sun} \approx 16°$), and P11 80/66 (Saturn encounter) is 0.97. The low A_{sun} value combined with long integration time causes larger uncertainty.

To test the effect of the Sun on the a_{Pc}, the calculation was repeated with the Sun excluded (a_{Psun}). Figure 3 shows the a_{Pc} values versus the D for the spacecraft from Figure 1 and a_{Psun}. The effect of the Sun is to cause the annual variation of the a_{Pc}. Therefore, the cause of the PA is also the cause of the annual periodicity.

Difference of the a_P between the spacecrafts

The P10 data included one of nine dates (≈ 0.11) with A_{sun} < 60° and five of nine dates (≈ 0.56) with A_{sun} > 120°. The P11 data included three of ten dates (≈ 0.30) with A_{sun} < 60° and four of ten dates (≈ 0.40) with A_{sun} > 120°. Figure 3 shows the trend of the a_{Psun} versus the D between P10 and P11 data points. At D > 10 AU, the a_{Psun} appears to be a linear function of D. At D < 10 AU, the Sun's influence is to lower a_{P11} more than a_{P10}.

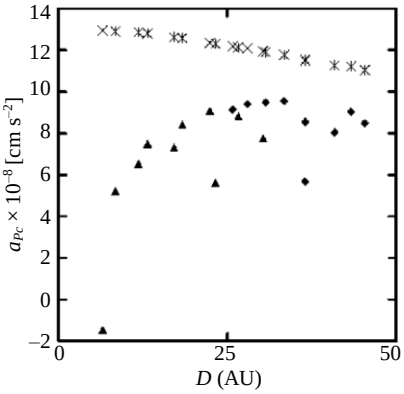

Fig. 3. The plots of the a_{Pc} data versus the geocentric distance D for P10 (solid diamonds) and P11 (solid triangles). The stars plot the data points for the a_{Pc} with the Sun excluded (a_{Psun}).

The SPM also suggests the mass of the planets and the mass of the galaxy has an influence on the ρ field. Figure 4 plots the a_{Pc} for the spacecraft, the a_{Pc} excluding the outer planets ($a_{Pplanets}$), and the a_{Pc} excluding the galaxy mass (a_{Pgal}) versus the D.

Because the outer planets are opposite the Sun for P10, the effect of the planets on the a_{Pc} of P10 is less than P11. However, as the D of P11 increases, the $a_{Pplanets} \rightarrow a_{Pc}$.

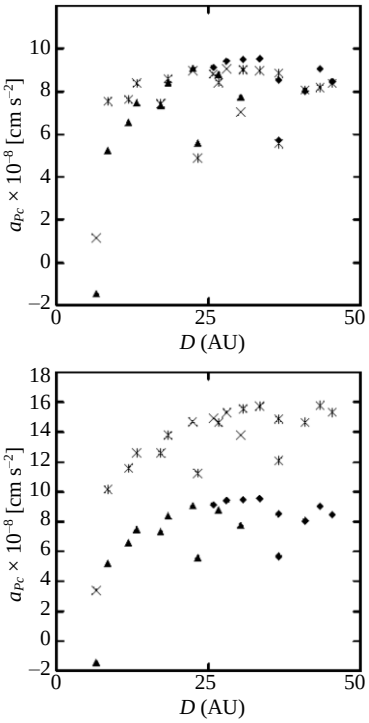

Fig. 4. The plots of the a_{Pc} versus the geocentric distance D for P10 (solid diamonds) and for P11 (solid triangles). The data points of the a_{Pc} excluding the outer planets a_{Pplanets} (upper figure), and the a_{Pc} excluding the galaxy mass a_{Pgal} (lower figure) are shown as stars.

From the galaxy scale perspective, the spacecraft in the solar system appears as near the large mass of the Sun and inner planets. The effect of the galaxy mass appears to decrease the a_{Pc} nearly uniformly for P11. The outer P10 data points show a trend to increasing relative effect of the galaxy mass. The orbit of P10 is closer to the Sun-Sgr.A* axis than P11 and the D of P10 is greater than the D of P11. However, this effect is within the uncertainty level.

The difference in a_{P10} and a_{P11} noted by Anderson *et al.* (2002) results primarily from the effect of the Sun. A secondary effect is the effect caused by increasing the D and a small effect of the planets on P11 which declines as the D increases. The SPM expects the galaxy mass to have a small difference between a_{P10} and a_{P11} caused by their different travel directions. The a_P is not constant as the CHASMP software assumed (Anderson *et al.*, 2002). Therefore, the varying a_P may explain the difference between the Sigma and CHASMP program methods for P10 (I) and their closer agreement at P10 (III) (Anderson *et al.*, 2002, Table 1).

Slow decline in the a_P

The plot shown in Figure 3 suggests that $\mathrm{d}a_{\text{Psun}}/\mathrm{d}D$ at $D <$ 10 AU is nearly zero, followed by a decline and then a flattening.

The radio signal measurements are from and to the Earth. At small values of the D, the relative effect of the Sun-Earth distance is larger than at farther D. As the D increases, the Solar System effect appears to approach a single mass located at the barycenter of the Solar System. Therefore, the a_P declines and approaches a constant value dictated by $\rho \propto -R^{-1}$. However, the SPM expects that at much greater D, the effect of the galaxy mass will increase to cause a difference in the a_P values between the spacecrafts.

Saturn encounter

Figure 5 shows the plot of the a_{Pc} versus the hours from the closest approach of P11 to the Saturn on P11 79/244 ($A_{\text{sun}} \approx 8°$). The plot shows the a_{Pc} varies widely over a period of hours. The negative a_{Pc} is a redshift. As seen in Figure 1, the SPM is consistent with the P11 77//270 ($A_{\text{sun}} \approx 43°$) data point at the beginning of the Saturn encounter of a near zero blueshift.

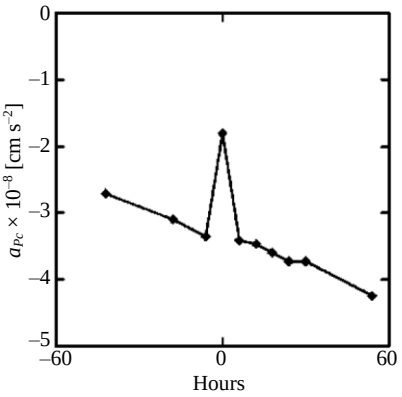

Fig. 5. The plot of the a_{Pc} versus the hours from the closest approach of P11 to the Saturn.

Large uncertainty of P11 80/66

Because the P11 80/66 ($A_{\text{sun}} \approx 166°$) data point extends over a relatively long time, the rapidly varying a_{Pc} seen in Figure 5 is consistent with the uncertainty in the P11 80/66 data point.

The a_{Psun} data points for P11 77/270 and P11 80/66 shown in Figure 3 have only a slightly lower slope than the later data points. The planets gravity well is in a larger gravity well of the Sun, which is in an even larger galaxy gravity well. The change from the Sun ρ versus D curve to a planet gravity well causes a smaller $K_{\text{f}}F$ term relative to $K_{\text{p}}P$. Table 2 lists $|K_{\text{f}}F| < |K_{\text{p}}P|$ for the P11 77/270, where "| |" means "absolute value", and $|K_{\text{f}}F| > |K_{\text{p}}P|$ for other data points. Without the Sun gravity well in the calculations, $|K_{\text{f}}F| > |K_{\text{p}}P|$ for all data points. Therefore, the a_{Psun} for the P11 77/270 data point is consistent with the other data points.

Cosmological connection

The SPM obtains the H_o value by $z \rightarrow \exp(-X) - 1 \approx -X$, where $X < 0$ in (Hodge, 2006) and $X > 0$ in this paper. Figure 6 shows the plot of D_l with the units changed to Mpc versus X. The straight line is a plot of the least-squares fit of the data. The line is

$$D_l = (2800 \pm 200\text{Mpc})X + (5 \pm 2) \times 10^{-11}\text{Mpc} \approx -\frac{c}{H_o} z \quad (5)$$

at 1σ and with a correlation coefficient of 0.95, where $H_o = 106 \pm 8$ km s^{-1} Mpc^{-1}.

The PA and the z of cosmology are the result of the same ρ effect on light. In the cosmological z calculation, the z follows the Hubble law if $\rho \propto R^{-1}$. In the gravity well, the z follows the negative Hubble law if $\rho \propto -R^{-1}$. The presence of other galaxies near the path of the light causes P and F variation of z. This is also the effect of matter close to the LOS in the PA. In the SPM, the Hubble law and $a_P \approx cH_o$ are manifestations of the Newtonian spherical property.

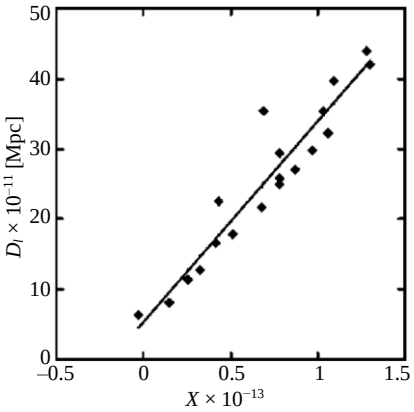

Fig. 6. The plot of the light travel distance D_l ($\times 10^{-11}$ Mpc) versus X ($\times 10^{-13}$) for both the spacecrafts. The line is a plot of $D_l = 2800X + 5 \times 10^{-11}$ Mpc.

DISCUSSION AND CONCLUSION

The variation of a_P through the sidereal day remains to be investigated. The specific location on the Earth relative to the Earth's center and the timing of the transmitting and receiving signals are required. The observation that the period is a sidereal day rather than a solar day suggests the SPM will be consistent with this observation, also.

The K values were calculated using data obtained in "interesting" environments. This means the ρ field was changing rapidly and long integration times were used. The K values can be calculated more accurately with longer integration time and in environments with little change in the ρ field. That is, the K values can be calculated more accurately in "uninterseting" environments when the Sun and the planets are farther from the LOS or by using shorter integration times.

The D at which the a_{Pgal} becomes noticeable is curiously close to the orbit of the Pluto.

Near planetary bodies the deep gravitational potential well causes a net frequency change of such a low value as to be undetectable. Because the mass of the spacecraft is much smaller than planetary bodies, the very small potential well of the spacecraft allows an observable frequency shift.

This SPM of the PA is that the frequency shift is always present and was present at less than 10 AU. However, as noted in the P11 77/270 data point and in the Saturn encounter calculation (Figure 5), the value of the a_P changes and may be a redshift. Therefore, further analysis of the spacecraft data can be a test of this model with additional caveats that a shorter integration period be used, that $A_{sun} \approx 180° \pm 30°$, and that the a_P be considered a variable (the Sigma software). The Jupiter to Saturn travel period with a minimal radial movement would reduce the Doppler effect. Because this model is a non-Doppler frequency shift model, the verification of this effect has significant cosmological implications.

The SPM suggests gravity is a manifestation of a curved ρ field. Sources, Sinks, and matter produce the curvature. In GR, matter curves Space and curved Space constrains the dynamics of matter. (The uppercase "S" on Space indicates the view of the GR and the ρ field of the SPM. A lower case "s" indicates the neutral backdrop, the Euclidean space.) In the SPM, the ρ field acts like the Space of the GR and space is a neutral backdrop (flat) in which distance is calculated using timing events such as using Cepheid stars. Therefore, the proposition that matter warps the ρ field is reasonable. Space in the GR and the ρ field in the SPM is curved, ubiquitous, and corporeal. Therefore, the objection to the Newtonian mechanics of "action at a distance" is removed. Calling the stuff of the ρ field "Space" as the GR does is tempting but confusing when dealing with the Euclidean, neutral backdrop type of space.

Hodge (2006) suggests the flow of the ρ field from Sources to Sinks causes the cell structure of galaxy clusters. An analogy is fluid flow from Sources to Sinks causes a Rankine oval. The B band luminosity L of a galaxies indicated the effect of a Source or Sink on the intergalactic redshift. In the redshift calculation, the use of L may also be the net effect of the Sources and Sinks and of the matter around galaxies. A problem with this

interpretation is that at the outer part of the galaxy, the gravitational mass of the galaxy is still larger than the ρ field effect as evidenced by the net attraction of hydrogen. Also, the L was found to be proportional to spiral galaxy rotation curve parameters (Hodge, 2022. Scalar potential model of spiral galaxy HI rotation curves and rotation curve asymmetry. Canadian Journal of Pure and Applied Sciences. 16(2):In Press) and to galaxy central parameters (Hodge, 2022. Scalar potential model of galaxy central mass and central velocity dispersion. Canadian Journal of Pure and Applied Sciences. 16(3):In Press) that do not include the total mass of the galaxy. The paradox between the two uses of L may be resolved if the effect of galaxy matter on intergalactic scales is zero. In fluid flow, an object placed in an otherwise unconstrained flow produces local turbulence downstream. However, eventually the flow of the fluid appears as if the object was absent. This is consistent with the presence of high metallicity matter in the intergalactic medium (Aracil *et al*., 2006). Therefore, the proposition that matter is neither a Source nor a Sink is consistent with the cluster and galaxy observations. Further, if the ρ field is flat, $\nabla\rho = 0$ and there is no flow. In such a condition such as between galaxy clusters, the static field of matter extends throughout the flat field.

The observations confirming the GR also confirm the ρ field effect because each has the same effect on matter. Gravitational lensing is the effect of the ρ field on photons perpendicular to their travel path. The effect herein is the effect of the ρ field on photons along their travel path. When observations consider matter that moves through space such as z measurements and gravitational lensing observations, the amount, curvature, and flow of the ρ field must be considered.

The author speculates that the GR corresponds to the SPM in the limit in which the Sources and Sinks may be replaced by a flat and static ρ field such as between cluster cells and on the Solar System scale at a relatively large distance from a Source or Sink. On the galaxy and galaxy cluster scale the ρ field is significantly curved from the proximity of Sources and Sinks and the GR fails (Sellwood and Kosowsky, 2001).

For a sample of 19 data points with published Pioneer Anomaly "acceleration" values, the SPM was found to be consistent with the observation of not only the value of the Pioneer Anomaly but also with the subtler effects noted by Anderson *et al*. (2002). The SPM is consistent with the general value of the a_P; with the annual periodicity; with the differing a_P between the spacecrafts; with the discrepancy between Sigma and CHASMP programs at P10 (I) and their closer agreement at P10 (III); with the slowly declining a_P; with the low value of the a_P immediately before the P11's Saturn encounter; with the high uncertainty in the value of the a_P obtained during and after the P11's Saturn encounter; and with the cosmological connection suggested by $a_P \approx cH_o$. The SPM has outstanding correlation to the observed data when the long integration time combined with rapidly changing ρ field is insignificant. Because the gradient of the ρ field produces a force on matter, the effect of the ρ field warp appears as the curvature of space proposed by the GR that causes the gravitational potential of matter.

ACKNOWLEDGMENT

The anonymous reviewer of Hodge (2006) inspired this investigation of the Pioneer Anomaly within the context of the SPM. The author acknowledges and appreciates the financial support of Maynard Clark, Apollo Beach, Florida, while the author was working on this project.

REFERENCES

Anderson, JD., Laing, PA., Lau, EL., Liu, AS., Nieto, MM. and Turyshev, SG. 2002. Study of the anomalous acceleration of Pioneer 10 and 11. Physical Review D. 65(8):082004. DOI: https://doi.org/10.1103/PhysRevD.65.082004.

Aracil, B., Tripp, TM., Bowen, DV., Prochaska, JX., Chen HW. and Frye, BL. 2006. High-metallicity, photoionized gas in intergalactic large-scale filaments. Monthly Notices of the Royal Astronomical Society. 367(1):139-155. DOI: https://doi.org/10.1111/j.1365-2966.2005.09962.x

Bertolami, O. and Páramos, J. 2004. The pioneer anomaly in the context of the braneworld scenario. Classical and Quantum Gravity. 21(13):3309-3321. DOI: https://doi.org/10.1088/0264-9381/21/13/013

Cooperstock, FI., Faraoni, V. and Vollick, DN. 1998. The influence of the cosmological expansion on local systems. The Astrophysical Journal. 503(1):61-66. DOI: https://doi.org/10.1086/305956.

Hodge, JC. 2006. Scalar potential model of redshift and discrete redshift. New Astronomy. 11(5):344-358. DOI: https://doi.org/10.1016/j.newast.2005.09.002.

Iorio, L. and Gioudice, G. 2006. What do the orbital motions of the outer planets of the Solar System tell us about the Pioneer anomaly? New Astronomy. 11(8):600-607. DOI: https://doi.org/10.1016/j.newast.2006.04.001

Nieto, MM. and Anderson, JD. 2005. Using early data to illuminate the Pioneer anomaly. Classical and Quantum Gravity. 22(24):5343-5354. DOI: https://doi.org/10.1088/0264-9381/22/24/008.

Nieto, MM., Turyshev, SG. and Anderson, JD. 2005. The Pioneer anomaly: The data, its meaning, and a future test.

AIP Conference Proceedings. 758(1):113-128; DOI: https://doi.org/10.1063/1.1900511

Sellwood, JA. and Kosowsky, A. 2001. Does dark matter exist? In: Gas and Galaxy Evolution. Eds. Hibbard, JE., Rupen, MP. and van Gorkom, JH. ASP Conference Series 240 (Astronomical Society of the Pacific, San Francisco, USA). pp.311-318. DOI: https://doi.org/10.48550/arXiv.astro-ph/0009074

Teplitz, VL., Stern, SA., Anderson, JD., Rosenbaum, D., Scalise, RJ. and Wentzler, P. 1999. Infrared Kuiper Belt constraints. The Astrophysical Journal. 516(1):425-435.

Toth, VT. and Turyshev, SG. 2006. The Pioneer anomaly: Seeking an explanation in newly recovered data. Canadian Journal of Physics. 84(12):1029-1047. DOI: https://doi.org/10.1139/P07-005

Turyshev, SG., Anderson, JD., Laing, PA., Lau, EL., Liu, AS. and Nieto, MM. 1999. The apparent anomalous, weak, long-range acceleration of Pioneer 10 and 11. XXXIV-th Rencontres de Moriond Meeting on Gravitational Waves and Experimental Gravity. Les Arcs, Savoi, France, January 23-30, 1999. pp.481-486. DOI: https://doi.org/10.48550/arXiv.gr-qc/9903024.

Received: April 12, 2022: Accepted: May 19, 2022